# Probe of topological invariants using quantum walks of a trapped ion in coherent state space*

Ya Meng(蒙雅)[1,2], Feng Mei(梅锋)[1,2,†], Gang Chen(陈刚)[1,2,3,‡], and Suo-Tang Jia(贾锁堂)[1,2]

[1] *State Key Laboratory of Quantum Optics and Quantum Optics Devices, Institute of Laser Spectroscopy, Shanxi University, Taiyuan* 030006, *China*
[2] *Collaborative Innovation Center of Extreme Optics, Shanxi University, Taiyuan* 030006, *China*
[3] *Collaborative Innovation Center of Light Manipulations and Applications, Shandong Normal University, Jinan* 250358, *China*

(Received 25 February 2020; revised manuscript received 6 April 2020; accepted manuscript online 12 April 2020)

We present a protocol to realize topological discrete-time quantum walks, which comprise a sequence of spin-dependent flipping displacement operations and quantum coin tossing operations, with a single trapped ion. It is demonstrated that the information of bulk topological invariants can be extracted by measuring the average projective phonon number when the walk takes place in coherent state space. Interestingly, the specific chiral symmetry owned by our discrete-time quantum walks simplifies the measuring process. Furthermore, we prove the robustness of such bulk topological invariants by introducing dynamical disorder and decoherence. Our work provides a simple method to measure bulk topological features in discrete-time quantum walks, which can be experimentally realized in the system of single trapped ions.

**Keywords:** topological quantum walk, topological invariant, trapped ion, coherent state space

**PACS:** 05.40.Fb, 03.67.Ac, 03.65.Vf, 37.10.Vz **DOI:** 10.1088/1674-1056/ab8893

## 1. Introduction

Topological physics, which exhibit some of the most striking phenomena in modern physics, have been investigated intensively in recent years.[1–3] Contrast to the conventional phases characterized by local order parameters, the bulk topological phases are distinguished by topologically invariant integers.[4] Classification and detection of bulk topological phases give an essential understanding of topological physics. In addition, the novel bulk topological features have potential important applications in quantum information for their robustness. Besides condensed-matter materials such as topological insulators and superconductors, topological phenomena also emerge in synthetic systems such as photonic systems[5–7] and cold atoms in optical lattices.[8] Moreover, recent progress has focused on the measurement of bulk topological invariants of these synthetic systems.[9–14] The flexibility offered by these synthetic simulators guarantees the exciting possibility of extending the study of topological matters to regimes beyond the scope of the condensed-matter physics based on electronic systems.

An outstanding example here is the identification of topological phenomena in discrete-time quantum walks (DTQWs), in which the movement of the particle (walker) on a lattice depends on the specific internal (coin) state.[15] The DTQW provides an unique platform to investigate all topological phases in one- and two-dimensional noninteraction systems with certain symmetries.[16,17] Over the past few years, it has become technologically possible to implement DTQWs in real systems using ultracold atoms in optical lattices,[18,19] trapped ions,[20,21] photons[22,23] and nuclear magnetic resonance.[24] Moreover, the topological effects, including the topological edge states, the topological phase transitions and the topological invariants, in the context of DTQWs have been widely discussed theoretically,[16,17,25–36] and experimentally measured by several groups.[37–51] For chiral DTQWs, the mean chiral displacement is proportional to the topological invariant in long-time limit.[39] For general DTQWs, the topological invariants can be obtained using scattering theory.[40] Furthermore, the topological invariants can also be directly extracted through the accumulated Berry phase of Bloch oscillating DTQWs in a circuit quantum electrodynamics (c-QED) architecture,[35,41] or through the winding number of a large-scale chiral DTQW.[42] Nevertheless, the direct measurement of these topological invariants is still a huge challenge for the experimental technology of tomography required by current experimental methods. Even the mean chiral displacement also requires the detection of all position states and the coin state at each lattice. Recently, a theoretical work proposed that the average photon number can be used to reveal the topological phases transition in a c-QED architecture, where a DTQW

*Project supported by the National Key R&D Program of China (Grant No. 2017YFA0304203), the National Natural National Science Foundation of China (Grant Nos. 11604392 and 11674200), the Changjiang Scholars and Innovative Research Team in Universities of Ministry of Education of China (Grant No. IRT_17R70), the Fund for Shanxi "1331 Project" Key Subjects Construction, and the 111 Project, China (Grant No. D18001).

†Corresponding author. E-mail: meifeng@sxu.edu.cn
‡Corresponding author. E-mail: chengang971@163.com

 

takes place in coherent state space.[52] The measurement of bulk topological invariants have also been discussed in this work, while it has no generality since the dependence of the initial coin state. In addition, all the above experimental progresses are based on photonic DTQWs, there are few studies on the topological features in other synthetic quantum systems.

In this paper, we propose an experimental protocol to realize topological DTQWs in coherent state space with single trapped ions. Through analytical and numerical analysis, we illuminate the topological structure of our DTQWs, including two pairs of topological invariants and the mean chiral displacements. More importantly, we demonstrate that the information of bulk topological invariants can be extracted through the average projective phonon number of the final state, with no need for reading out the position states and the coin state at each lattice. For completeness, we define two kinds of average projective phonon numbers corresponding to different parameter regions. By introducing dynamical disorder and decoherence, we verify the robustness of our results. This work gives a simple method to directly measure bulk topological invariants in discrete-time quantum dynamics in coherent state space.

This paper is structured as follows. In Section 2, we present a protocol to realize a spin-dependent flipping operation in coherent state space with a single trapped ion. In Section 3, we show the forms of our DTQWs in the system of single trapped ions and analyze the topological structure of such DTQWs. In Section 4, we derive two kinds of average projective phonon numbers, which contain the information of bulk topological invariants. Furthermore, we demonstrate the robustness of our results by introducing dynamical disorder and decoherence. Finally, we summarize in Section 5.

## 2. Spin-dependent flipping displacement operation

The key problem of realizing DTQWs in real systems is how to implement a spin-dependent displacement operation. Here we implement a spin-dependent flipping displacement operation in coherent state space with a single trapped ion. Most of the previous works are concerned with the spin-dependent displacement operation without flipping. Only one experimental group considers a complicated spin-dependent flipping displacement operation, which is implemented by a special q-plate.[38,39] Although this seems like a small difference, it can have far reaching consequences with a simple chiral symmetry, as we will show in the following.

The spin-dependent flipping displacement operation is defined as

$$T_{\uparrow\downarrow}^{\alpha} = \sum_{x} |(x+1)\alpha\rangle\langle x\alpha| \otimes |\uparrow\rangle\langle\downarrow| + |(x-1)\alpha\rangle\langle x\alpha| \otimes |\downarrow\rangle\langle\uparrow|, \tag{1}$$

where the positions of the walker (ion) are encoded with a series of coherent states $|x\alpha\rangle$, and the coin states ($|\uparrow\rangle$, $|\downarrow\rangle$) denote two ground-state hyperfine levels of the ion. This spin-dependent flipping displacement operation can be realized through a pulse sequence in the system of single trapped ion.

Firstly, we apply displacement Raman beams, the corresponding interaction Hamiltonian between the light field and the trapped ion in the interaction frame can be written as[53]

$$\begin{aligned} H_{\mathrm{I}}(t) = {} & \Omega_{\downarrow} \mathrm{e}^{-\mathrm{i}\delta t} \exp[\mathrm{i}\eta(a\,\mathrm{e}^{-\mathrm{i}\omega_z t} + a^{\dagger}\,\mathrm{e}^{\mathrm{i}\omega_z t})] |\downarrow\rangle\langle\downarrow| \\ & + \Omega_{\uparrow} \mathrm{e}^{-\mathrm{i}\delta t} \exp[\mathrm{i}\eta(a\,\mathrm{e}^{-\mathrm{i}\omega_z t} + a^{\dagger}\,\mathrm{e}^{\mathrm{i}\omega_z t})] |\uparrow\rangle\langle\uparrow| \\ & + \mathrm{H.c.}, \end{aligned} \tag{2}$$

where $\Omega_{\uparrow}$ ($\Omega_{\downarrow}$) is the Rabi frequency when the coin state is $|\uparrow\rangle$ ($|\downarrow\rangle$), $\eta$ is the Lamb–Dicke parameter, $\delta$ is the frequency difference of the displacement Raman beams, $\omega_z$ is the ion's motional mode frequency, and $a^{\dagger}$ ($a$) is the creation (annihilation) operator of phonon. In the Lamb–Dicke limit ($\eta \ll 1$), the resulting Hamiltonian is given by

$$\begin{aligned} H_{\mathrm{I}} \simeq {} & (\mathrm{i}\eta\Omega_{\downarrow}a^{\dagger} - \mathrm{i}\eta\Omega_{\downarrow}^{*}a) |\downarrow\rangle\langle\downarrow| \\ & + (\mathrm{i}\eta\Omega_{\uparrow}a^{\dagger} - \mathrm{i}\eta\Omega_{\uparrow}^{*}a) |\uparrow\rangle\langle\uparrow|, \end{aligned} \tag{3}$$

where we assume $\delta = \omega_z$, and replace the fast oscillating terms by their zero average values. Thus, the evolution operator $\mathcal{U}$ of the interaction Hamiltonian over time $\delta t$ can act as a displacement operator,

$$\mathcal{U} = D(\Omega_{\downarrow}\eta\,\delta t) |\downarrow\rangle\langle\downarrow| + D(\Omega_{\uparrow}\eta\,\delta t) |\uparrow\rangle\langle\uparrow|, \tag{4}$$

where $D(\beta) = \exp(\beta a^{\dagger} - \beta^{*}a)$. It is clear that Eq. (4) will be essentially a displacement of $\Omega_{\uparrow}\eta\,\delta t$ or $\Omega_{\downarrow}\eta\,\delta t$ if the coin state is $\uparrow$ or $\downarrow$, respectively.

Secondly, a $\pi$ pulse $R_{\pi}$, which exchanges the two coin states, is required.

Finally, we apply displacement Raman beams again with opposite Rabi frequencies, the resulting evolution operator over time $\delta t$ is

$$\mathcal{U}^{\dagger} = D(-\Omega_{\downarrow}\eta\,\delta t) |\downarrow\rangle\langle\downarrow| + D(-\Omega_{\uparrow}\eta\,\delta t) |\uparrow\rangle\langle\uparrow|. \tag{5}$$

Equation (5) will be a displacement of $-\Omega_{\uparrow}\eta\,\delta t$ or $-\Omega_{\downarrow}\eta\,\delta t$ if the coin state is $\uparrow$ or $\downarrow$, respectively. Application of this pulse sequence generates a total evolution

$$D(\alpha) |\uparrow\rangle\langle\downarrow| + D(-\alpha) |\downarrow\rangle\langle\uparrow|, \tag{6}$$

which exactly corresponds to the spin-dependent flipping displacement operation $T^{\alpha}_{\uparrow\downarrow}$ with identical leftward and rightward step size $\alpha \sim (\Omega_{\downarrow} - \Omega_{\uparrow})\eta\,\delta t$, see Fig. 1. In order to make the walk of different spins in the opposite directions in coherent state space, which is the core in quantum walks, we require that the Rabi frequencies are opposite.

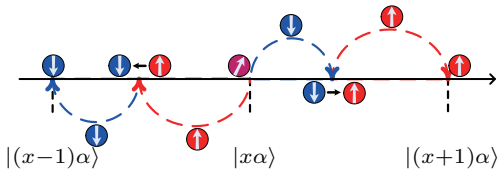


**Fig. 1.** The diagram of the spin-dependent flipping translation $T^{\alpha}_{\uparrow\downarrow} = \mathcal{U}^{\dagger}R_{\pi}\mathcal{U}$ in the system of a trapped ion. The interaction of the displacement Raman beams and the trapped ion allow the coherent displacements in coherent state space. Between two displacement Raman beams, a $\pi$ pulse, which exchanges the spin, is required. In this diagram, the Rabi frequencies satisfy $\Omega_{\uparrow} = -\frac{3}{2}\Omega_{\downarrow}$ as an example.

Based on the current ion-trap techniques,[20,21] it is possible to realize such a spin-dependent flipping displacement operation in the realistic ion-trap experiments. For example, the Rabi frequencies can satisfy $\Omega_{\uparrow} = -\frac{3}{2}\Omega_{\downarrow}$ with $\Omega_{\downarrow} = 2\pi \times 68$ kHz by choosing appropriate polarization and directions of Raman beams.[20,21,53,59] With the Lamb–Dicke parameter $\eta = 0.06$,[21] different step sizes ($\alpha = 0.3, 0.5, 1.5$) of the spin-dependent flipping displacement operation can be realized by choosing different durations of Raman beams ($\delta t = 5$ μs, 8 μs, 24 μs). Within the decoherence time of the motional mode,[60] the spin-dependent flipping displacement operation can be repeated many times for realizing multistep DTQWs as we show in the following. In addition, the quantum coin tossing operations, which act on the internal state of the walker, are also required for realizing DTQWs. In this paper, we consider a specific quantum coin tossing operation $R_x(2\theta) = \mathrm{e}^{-\mathrm{i}\theta\sigma_x}$, which can be easily performed by a resonant radio frequency pulse.[20]

## 3. Topological invariants

Since in Floquet 1D systems, there exists two independent classes of protected edge states at either 0 or $\pi$ energies. A complete topological classification for such a system with chiral symmetry would require introducing a pair of topological invariants $(\nu_0, \nu_{\pi})$.[26] Thus, we consider two inequivalent "chiral symmetry time frames" of DTQWs as follows:

$$U_1^{\alpha} = R_x\left(\frac{\theta_1}{2}\right)T^{\alpha}_{\uparrow\downarrow}R_x(\theta_2)T^{\alpha}_{\uparrow\downarrow}R_x\left(\frac{\theta_1}{2}\right), \tag{7}$$

$$U_2^{\alpha} = R_x\left(\frac{\theta_2}{2}\right)T^{\alpha}_{\uparrow\downarrow}R_x(\theta_1)T^{\alpha}_{\uparrow\downarrow}R_x\left(\frac{\theta_2}{2}\right). \tag{8}$$

The topological analysis of our DTQWs is based on coordinate space $|x\alpha\rangle \to |x\rangle$. Since the operators $U_1$ and $U_2$ in coordinate space have chiral symmetry with the symmetry operator $\Gamma = \sigma_z$, we rewrite the operators $U_{1,2}$ as

$$U_1 = \mathrm{e}^{-\mathrm{i}\pi}F\cdot\Gamma F^{\dagger}\Gamma = \mathrm{e}^{-\mathrm{i}\pi}\tilde{U}_1, \tag{9}$$

$$U_2 = \mathrm{e}^{-\mathrm{i}\pi}\Gamma F^{\dagger}\Gamma\cdot F = \mathrm{e}^{-\mathrm{i}\pi}\tilde{U}_2, \tag{10}$$

where $F = R_x(\theta_1/2)T_{\uparrow\downarrow}R_x(\theta_2/2)$. Thus, the complete topological invariants $(\nu_0, \nu_{\pi})$ for the operators $U_{1,2}$ can be obtained from the topological invariants $(\tilde{\nu}_0, \tilde{\nu}_{\pi})$ governed by the operators $\tilde{U}_{1,2}$ with the relation $(\nu_0, \nu_{\pi}) = (\tilde{\nu}_{\pi}, \tilde{\nu}_0) = (\frac{\tilde{\nu}_1 - \tilde{\nu}_2}{2}, \frac{\tilde{\nu}_1 + \tilde{\nu}_2}{2})$.[26,28] Furthermore, it is straightforward to show that the winding numbers $\tilde{\nu}_{1,2}$ obtained through the operators $\tilde{U}_{1,2}$ are equivalent to the winding number $\nu_{1,2}$ obtained through the operators $U_{1,2}$. Using the Fourier transformation $|x\rangle = 1/\sqrt{2\pi}\sum_k \mathrm{e}^{-\mathrm{i}kx}|k\rangle$, the spin-dependent flipping displacement operation can be written as $T_{\uparrow\downarrow}(k) = [0, \mathrm{e}^{-\mathrm{i}k}; \mathrm{e}^{\mathrm{i}k}, 0]$. According to the Floquet theory, the one step evolution operator can be written as $U_1 = \int_{-\pi}^{\pi}\mathrm{d}k\cdot U_1(k)\otimes|k\rangle\langle k| = \mathrm{e}^{-\mathrm{i}H_{\mathrm{eff}}}$. The effective Hamiltonian $H_{\mathrm{eff}}$ has the form

$$H_{\mathrm{eff}} = \int_{-\pi}^{\pi}\mathrm{d}k[E(k)\boldsymbol{n}(k)\cdot\boldsymbol{\sigma}]\otimes|k\rangle\langle k|, \tag{11}$$

where $\boldsymbol{\sigma} = (\sigma_x, \sigma_y, \sigma_z)$ is the vector of Pauli matrices, $E(k)$ and $\boldsymbol{n}(k)$ characterize the eigenvalues and the spinor eigenstates. It is straightforward to obtain

$$\begin{aligned}
\cos E(k) &= -\sin\frac{\theta_2}{2}\sin\frac{\theta_1}{2}\cos(2k) + \cos\frac{\theta_2}{2}\cos\frac{\theta_1}{2},\\
n_x(k) &= \frac{\sin\frac{\theta_2}{2}\cos\frac{\theta_1}{2}\cos(2k) + \cos\frac{\theta_2}{2}\sin\frac{\theta_1}{2}}{\sin E},\\
n_y(k) &= \frac{\sin\frac{\theta_2}{2}\sin(2k)}{\sin E},\\
n_z(k) &= 0.
\end{aligned} \tag{12}$$

The winding number is defined as

$$\nu_1 = \frac{1}{2\pi}\int_{-\pi}^{\pi}\mathrm{d}k\cdot\left(\boldsymbol{n}\times\frac{\partial\boldsymbol{n}}{\partial k}\right)\cdot\boldsymbol{A}, \tag{13}$$

where the vector $\boldsymbol{A} = (0,0,1)$ is perpendicular to $\boldsymbol{n}(k)$ for the whole first Brillouin zone. Similarly, we can obtain the winding number $\nu_2$. The difference in the winding number $\nu_0$ ($\nu_{\pi}$) on either side of the boundary is equal to the number of edge states with quasienergy 0 ($\pi$) on the boundary, which is the bulk-edge correspondence for DTQWs. We have numerically calculated the winding number $\nu_{1,2}$ and show the complete phase diagram in Fig. 2.

Without loss of generality, in the following discussion, $\theta_2$ is fixed to $3\pi/2$ and $\theta_1 \in [0, 2\pi]$ when we consider the topological invariants varying with the rotation angle, the transition points are at $\theta_1 = \pi/2$ and $3\pi/2$. We fix $\theta_1 = \pi/4, 3\pi/4$ and $\theta_2 = 3\pi/2$ when we consider the topological invariants as functions of the step $t$, see Fig. 2.

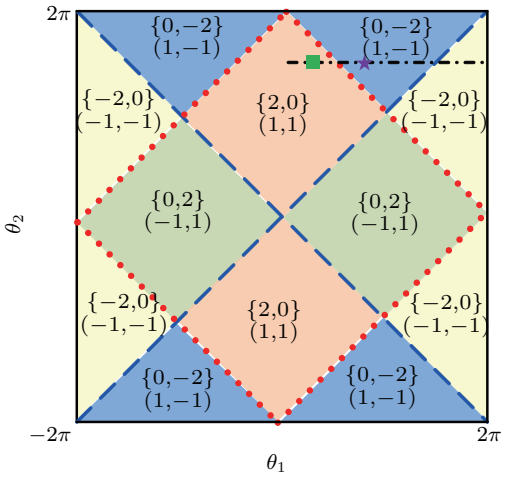


**Fig. 2.** The phase diagram governed by $U_{1,2}$. The DTQWs have effective Hamiltonians with gaps around both $\varepsilon = 0$ and $\varepsilon = \pi$, except at the gapless points where gaps close at $\varepsilon = 0$ (dashed) or $\varepsilon = \pi$ (dotted). For each gapped phase, the corresponding pair of winding numbers $\{\nu_1, \nu_2\}$ as well as the pair of topological invariants $(\nu_0, \nu_\pi)$ are shown. The dash-dotted line and the two symbols indicate the rotating parameters for detecting the topological invariants.

From the previous research,[39] the topological invariants can be obtained through the mean chiral displacement

$$\mathcal{C}(t) = \langle \Gamma x \rangle = \sum_x x(P_{x,+} - P_{x,-}), \tag{14}$$

where $P_{x,\pm} = |\langle x, \pm|\Psi(t)\rangle|^2$, $|\pm\rangle$ are the eigenstates of the chiral operator $\Gamma$ with the eigenvalues $\pm 1$, $|\Psi(t)\rangle$ is the final state after $t$ steps of a DTQW. In the long-time limit $t \to \infty$, the mean chiral displacement $\mathcal{C}$ becomes proportional to the winding number $\nu$,

$$\mathcal{C} \simeq \frac{\nu}{2}. \tag{15}$$

Therefore, the topological invariants $(\nu_0, \nu_\pi)$ can be directly obtained from the mean chiral displacements $\mathcal{C}_{1,2}$ with $(\nu_0, \nu_\pi) = (\mathcal{C}_1 - \mathcal{C}_2, \mathcal{C}_1 + \mathcal{C}_2)$.

In Fig. 3, we show the mean chiral displacements $\mathcal{C}_{1,2}$ and the associated mean chiral displacements $\mathcal{C}_1 \mp \mathcal{C}_2$ varying with the rotation angle $\theta_1$ and the step $t$, respectively. The walker is initially located at $|\Psi_0\rangle = |0\rangle \otimes |\uparrow\rangle$, where the different initial coin states have no influence on the behavior of the mean chiral displacements. Though the mean chiral displacements $\mathcal{C}_{1,2}$ (the associated mean chiral displacements $\mathcal{C}_1 \mp \mathcal{C}_2$) oscillate near the topological invariants $\nu_{1,2}/2$ ($\nu_{0,\pi}$) of the system, they are enough to have clear detections of the topological invariants since the centers of oscillation are always localized at the corresponding topological invariants, see Figs. 3(a) and 3(b). When we increase the step $t$, the mean chiral displacements $\mathcal{C}_{1,2}$ (the associated mean chiral displacements $\mathcal{C}_1 \mp \mathcal{C}_2$) will oscillate near the topological invariants $\nu_{1,2}/2$ ($\nu_{0,\pi}$) with decreasing oscillation amplitude, see Figs. 3(c) and 3(d).

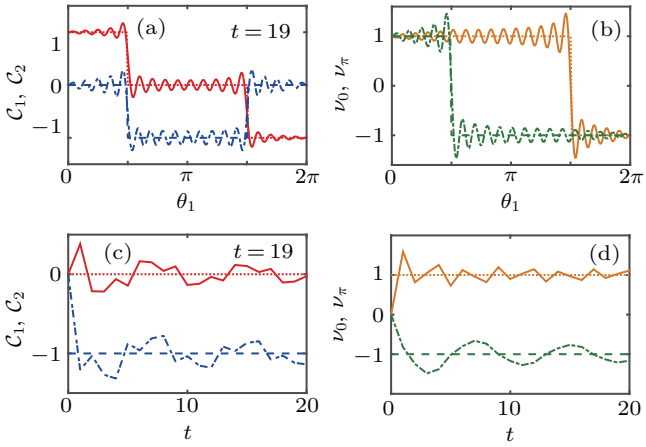


**Fig. 3.** (a), (c) The mean chiral displacements $\mathcal{C}_{1,2}$ varying as functions of the rotation angle $\theta_1$ and the step $t$ with $\theta_1 = 3\pi/4$, the rotation angle $\theta_2$ is fixed at $3\pi/2$. The solid (dash-dotted) line indicates the mean chiral displacement $\mathcal{C}_1$ ($\mathcal{C}_2$), and the dotted (dashed) line corresponds to the topological invariant $\nu_1/2$ ($\nu_2/2$) governed by $U_1$ ($U_2$). (c), (d) The associated mean chiral displacements $\mathcal{C}_1 \mp \mathcal{C}_2$ varying as functions of the rotation angle $\theta_1$ and the time step $t$ with $\theta_1 = 3\pi/4$, the rotation angle $\theta_2$ is fixed at $3\pi/2$. The solid (dash-dotted) line indicates the associated mean chiral displacement $\mathcal{C}_1 - \mathcal{C}_2$ ($\mathcal{C}_1 + \mathcal{C}_2$), and the dotted (dashed) line corresponds to the topological invariant $\nu_0$ ($\nu_\pi$) of our DTQWs.

## 4. Experimental detection of topological invariants

In ion-trap systems, the phonon number can be measured through Rabi flopping or blue-sideband driving,[53–55] and has been detected experimentally for revealing rich physical phenomena.[56–58] Here we illustrate that the information of bulk topological invariants can be extracted through the average projective phonon number of final state, which is convenient to measure in experiments. Since the following analysis are identical for these two DTQWs governed by $U_{1,2}^\alpha$, we only consider $U_1^\alpha$ for an example. We assume that the final state after $t$ steps of a DTQW has the form of $|\Psi_f^\alpha\rangle = (U_1^\alpha)^t |\Psi_0^\alpha\rangle = \Sigma_{x,\sigma} A_{x,\sigma} |x\alpha, \sigma\rangle$, where $\sigma$ is the spin index. We consider the average projective phonon numbers of the final state $N^\pm = \langle \Psi_f | a^\dagger a P_\pm | \Psi_f \rangle$, where $a^\dagger$ ($a$) is creation (annihilation) operator of phonon and $P_\pm = |\pm\rangle\langle\pm|$ are projective operators ($|\pm\rangle$ indicate the eigenstates of the chiral operator $\Gamma$). In our DTQWs, the eigenstates of the chiral operator $\Gamma$ are exactly the coin states $|\uparrow\rangle$ and $|\downarrow\rangle$. This simple chiral symmetry will make the measurement process more easier.

Thus, the average projective phonon numbers can be written as

$$\begin{aligned} N^{\uparrow\downarrow} &= \langle \Psi_f^\alpha | a^\dagger a P_{\uparrow\downarrow} | \Psi_f^\alpha \rangle \\ &= \sum_{x,x',\sigma,\sigma'} A_{x,\sigma}^* A_{x',\sigma'} \langle x\alpha, \sigma | (a^\dagger a \, |\uparrow\downarrow\rangle \langle\uparrow\downarrow|) | x'\alpha, \sigma' \rangle \\ &= \sum_{x,x'} x x' A_{x,\uparrow\downarrow}^* A_{x',\uparrow\downarrow} |\alpha|^2 \, \mathrm{e}^{-\frac{(x'-x)^2}{2}|\alpha|^2}. \end{aligned} \tag{16}$$

Get rid of the sum over $x'$, $N^{\uparrow\downarrow}$ can be rewritten as

$$N^{\uparrow\downarrow} = |\alpha|^2 \sum_x x^2 |A_{x,\uparrow\downarrow}|^2$$

$$+|\alpha|^2 \mathrm{e}^{-|\alpha|^2/2}\sum_x x(x+1)A^*_{x,\uparrow\downarrow}A_{x+1,\uparrow\downarrow}+\text{c.c.}$$
$$+|\alpha|^2 \mathrm{e}^{-2|\alpha|^2}\sum_x x(x+2)A^*_{x,\uparrow\downarrow}A_{x+2,\uparrow\downarrow}+\text{c.c.}$$
$$+\cdots, \tag{17}$$

where c.c. is complex conjugation. It is clear to see that the information of the mean chiral displacement $\mathcal{C}_1 = x(|A_{x,\uparrow}|^2 - |A_{x,\downarrow}|^2)$ is contained in $N^{\uparrow\downarrow}$.

In the following discussions, we show the details about how to extract the information of the mean chiral displacement $\mathcal{C}_1$ from the average projective phonon number. For completeness, we consider two cases corresponding to different regions of parameter $|\alpha|$.

### 4.1. The case when $|\alpha|$ is large

When $|\alpha|$ is large enough, the average projective phonon numbers have really simple expressions $N^{\uparrow\downarrow} = |\alpha|^2\sum_x x^2|A_{x,\uparrow\downarrow}|^2$, where only the first term in Eq. (17) contributes. We consider two DTQWs with different initial states, $|-m\alpha\rangle\otimes|\varphi_0\rangle$ and $|m\alpha\rangle\otimes|\varphi_0\rangle$, where $|\varphi_0\rangle$ is the initial coin state.

Thus, the average projective phonon numbers of these two DTQWs are

$$N_1^{\uparrow\downarrow} = |\alpha|^2\sum_x (x-m)^2|A_{x,\uparrow\downarrow}|^2,$$
$$N_2^{\uparrow\downarrow} = |\alpha|^2\sum_x (x+m)^2|A_{x,\uparrow\downarrow}|^2, \tag{18}$$

and the difference of the average projective phonon numbers is defined as

$$\Delta N = (N_2^{\uparrow}-N_1^{\uparrow})-(N_2^{\downarrow}-N_1^{\downarrow}) = 4m|\alpha|^2\sum_x x(|A_{x,\uparrow}|^2-|A_{x,\downarrow}|^2), \tag{19}$$

which is exactly proportional to $\mathcal{C}_1$.

In Fig. 4, we show the difference of the average projective phonon numbers $\Delta N$ as functions of the rotation angle $\theta_1$ and the step $t$. The initial states are prepared as $|\Psi_0^{\alpha}\rangle = |\pm 2\alpha\rangle\otimes|\uparrow\rangle$. When $|\alpha|$ is large, such as $|\alpha| = 1.5$, $\Delta N$ is exactly proportional to $\mathcal{C}_1$. However, if $|\alpha|$ is chosen smaller, such as $\alpha = 0.5$, $\Delta N$ will deviate from $\mathcal{C}_1$, see Figs. 4(a) and 4(b). That is, $\Delta N$ is a good observable quantity for characterizing the topological invariants when the parameter of the system $|\alpha|$ is large.

Furthermore, the novel topological features of a system are robust against small perturbations. Here, we verify the robustness of $\Delta N$ by introducing dynamical disorder and decoherence. For the situation with dynamical disorder,[39] the rotation angle $\theta_1$ is chosen randomly from the interval $[\bar{\theta}_1 - \frac{\pi}{20}, \bar{\theta}_1 + \frac{\pi}{20}]$ at every step of a DTQW, where $\bar{\theta}_1$ indicates the corresponding parameter without disorder. This small fluctuation on the rotation angle $\theta_1$ can be experimentally realized by controlling the duration of the radio frequency pulse.[20] After 50 times of independent DTQWs with dynamical disorder, the ensemble average of $\Delta N$ converges to the results without disorder, see Figs. 4(c) and 4(d). For the situation with decoherence,[21,53,59,61] we can randomize the phase between each step through a operator $U_{de} = \sum_x |x\rangle\langle x|\otimes \mathrm{e}^{\mathrm{i}\delta\sigma_z}$ with $\delta\in(-q\pi, q\pi)$. The parameter $q$ describes the strength of decoherence. After 50 times of independent DTQWs with decoherence $q = 0.1$, the ensemble average of $\Delta N$ also converges to the results without decoherence, see Figs. 4(e) and 4(f). Our numerical results show that $\Delta N$ is robust against small perturbations, such as dynamical disorder and decoherence.

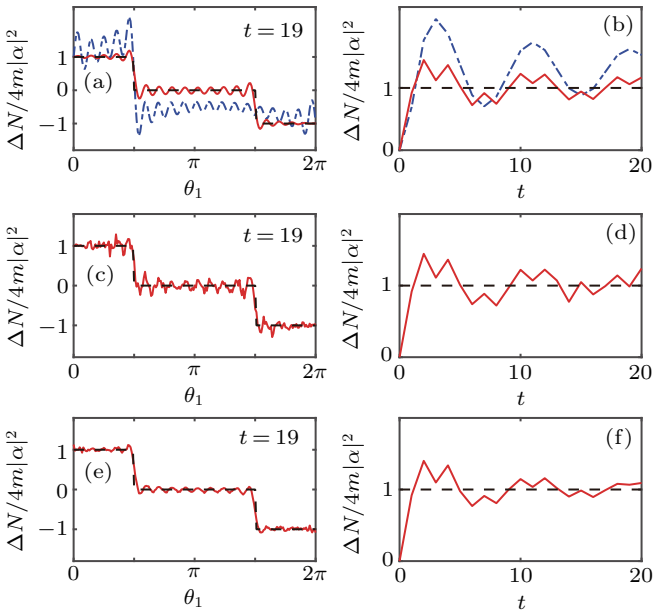


**Fig. 4.** The difference of the average projective phonon numbers $\Delta N$ governed by $U_1^{\alpha}$. The dashed lines correspond to the topological invariant $\nu_1/2$ of our DTQW governed by $U_1$. (a), (b) The difference of the average projective phonon numbers $\Delta N$ without dynamical disorder and decoherence, as functions of the rotation angle $\theta_1$ and the step $t$ with $\theta_1 = \pi/4$, the rotation angle $\theta_2$ is fixed at $3\pi/2$. The solid (dash-dotted) lines indicate $|\alpha| = 1.5$ (0.5). (c)–(f) The difference of the average projective phonon numbers $\Delta N$ with (c), (d) dynamical disorder or (e), (f) decoherence, as functions of the rotation angle $\theta_1$ or the step $t$ with $\theta_1 = \pi/4$, the rotation angle $\theta_2$ is fixed at $3\pi/2$ and $|\alpha| = 1.5$. The solid lines indicate the ensemble average over 50 times of DTQWs with dynamical disorder or decoherence.

### 4.2. The case when $|\alpha|$ is small

When $|\alpha|$ is small, the contributions of higher terms in Eq. (17) can not be neglected anymore. In this case, the difference of the average projective phonon numbers $\Delta N$ is not appropriate for characterizing the topological invariants. In order to find the new observable quantity, we consider modified one step unitary operators

$$\tilde{U}^{\alpha}_{1,2} = R_x(\theta_{1,2}/2)R_z(2\phi)T^{\alpha}_{\uparrow\downarrow}R_x(\theta_{2,1})R_z(2\phi)T^{\alpha}_{\uparrow\downarrow}R_x(\theta_{1,2}/2),$$

where $R_z(2\phi) = \mathrm{e}^{-\mathrm{i}\phi\sigma_z}$. The coin operator $R_z(\phi)$ is able to be easily performed in the system of single trapped ion, just like $R_x(\theta)$. Compared with $U^{\alpha}_{1,2}$, different phases can be accumu-

lated for different position states after $t$ steps of DTQWs governed by $\tilde{U}_{1,2}^{\alpha}$. We only consider $\tilde{U}_{1}^{\alpha}$ for an example. All of the following analyses are the same for $\tilde{U}_{2}^{\alpha}$. Thus, the new final state of system is $|\tilde{\Psi}_{f}^{\alpha}\rangle = (\tilde{U}_{1}^{\alpha})^{t}|\tilde{\Psi}_{0}^{\alpha}\rangle = \sum_{x,\sigma} \mathrm{e}^{\mathrm{i}x\phi} A_{x,\sigma}|x\alpha,\sigma\rangle$.

The average projective phonon numbers of the new final state have the form

$$\begin{aligned}\tilde{N}^{\uparrow\downarrow} &= |\alpha|^2 \sum_x x^2 |A_{x,\uparrow\downarrow}|^2 \\ &\quad + |\alpha|^2 \mathrm{e}^{-|\alpha|^2/2} \mathrm{e}^{\mathrm{i}\phi} \sum_x x(x+1) A_{x,\uparrow\downarrow}^{*} A_{x+1,\uparrow\downarrow} + \text{c.c.} \\ &\quad + |\alpha|^2 \mathrm{e}^{-2|\alpha|^2} \mathrm{e}^{\mathrm{i}2\phi} \sum_x x(x+2) A_{x,\uparrow\downarrow}^{*} A_{x+2,\uparrow\downarrow} + \text{c.c.} \\ &\quad + \cdots . \end{aligned} \tag{20}$$

When the step of DTQW $t \to \infty$, $\tilde{N}^{\uparrow\downarrow}$ can be rewritten in another form

$$\begin{aligned}\tilde{N}^{\uparrow\downarrow} &= |\alpha|^2 \sum_x x^2 |A_{x,\uparrow\downarrow}|^2 \\ &\quad - 2\cos(2\phi)|\alpha|^2 \mathrm{e}^{-2|\alpha|^2} \mathcal{L}^{\uparrow\downarrow}(2) t^2 \\ &\quad - 2\cos(4\phi)|\alpha|^2 \mathrm{e}^{-8|\alpha|^2} \mathcal{L}^{\uparrow\downarrow}(4) t^2 \\ &\quad - \cdots , \end{aligned} \tag{21}$$

where $\mathcal{L}^{\uparrow\downarrow}(m) \approx \int_{-\pi}^{\pi} \frac{\mathrm{d}k}{\pi} \frac{-\sin^2(\theta_1/2)\sin^2(2k)\cos(mk)}{2-[\sin(\theta_1/2)\cos(2k)+\cos(\theta_1/2)]^2}$. We note that $\mathcal{L}^{\uparrow\downarrow}(m = \text{odd}) = 0$. The detailed derivation of Eq. (21) will be shown in Appendix A.

Here, we consider the second and fourth terms, ignoring the more higher terms. For extracting $\mathcal{C}_1$ from $\tilde{N}^{\uparrow\downarrow}$, two groups of DTQWs are required. Each group contains two walks with same initial state while $\phi = \pi/8$, $3\pi/8$, respectively. For the first group, the initial state is $|-m\alpha\rangle \otimes |\varphi_0\rangle$. As for the second, we just change the initial state into $|m\alpha\rangle \otimes |\varphi_0\rangle$. The average projective phonon numbers of these four walks are

$$\begin{aligned}\tilde{N}_{1,2}^{\uparrow\downarrow}\left(\phi = \frac{\pi}{8}\right) &= |\alpha|^2 \sum_x (x \mp m)^2 |A_{x,\uparrow\downarrow}|^2 \\ &\quad - \sqrt{2}|\alpha|^2 \mathrm{e}^{-2|\alpha|^2} \mathcal{L}^{\uparrow\downarrow}(2) t^2, \end{aligned} \tag{22}$$

$$\begin{aligned}\tilde{N}_{1,2}^{\uparrow\downarrow}\left(\phi = \frac{3\pi}{8}\right) &= |\alpha|^2 \sum_x (x \mp m)^2 |A_{x,\uparrow\downarrow}|^2 \\ &\quad + \sqrt{2}|\alpha|^2 \mathrm{e}^{-2|\alpha|^2} \mathcal{L}^{\uparrow\downarrow}(2) t^2. \end{aligned} \tag{23}$$

We define the combination of these average projective phonon numbers as

$$\begin{aligned}\delta\tilde{N}^{\uparrow\downarrow} &= \left[\tilde{N}_{2}^{\uparrow\downarrow}\left(\phi = \frac{\pi}{8}\right) + \tilde{N}_{2}^{\uparrow\downarrow}\left(\phi = \frac{3\pi}{8}\right)\right] \\ &\quad - \left[\tilde{N}_{1}^{\uparrow\downarrow}\left(\phi = \frac{\pi}{8}\right) + \tilde{N}_{1}^{\uparrow\downarrow}\left(\phi = \frac{3\pi}{8}\right)\right], \end{aligned} \tag{24}$$

and we have

$$\begin{aligned}\delta\tilde{N} &= \delta\tilde{N}^{\uparrow} - \delta\tilde{N}^{\downarrow} \\ &= 8m|\alpha|^2 \sum_x x(|A_{x,\uparrow}|^2 - |A_{x,\downarrow}|^2), \end{aligned} \tag{25}$$

which is exactly proportional to $\mathcal{C}_1$. By now, we find the new observable quantity to characterize the topological invariants when $|\alpha|$ is small.

Using a numerical simulation, we demonstrate that the combination of the average projective phonon numbers $\delta\tilde{N}$ agree fairly well with $\mathcal{C}_1$. In Fig. 5, we show $\delta\tilde{N}$ governed by $\tilde{U}_{1}^{\alpha}$ as functions of the rotation angle $\theta_1$ and the step $t$. The initial states are prepared as $|\tilde{\Psi}_{0}^{\alpha}\rangle = |\pm 2\alpha\rangle \otimes |\uparrow\rangle$. It is clear that $\delta\tilde{N}$ is exactly proportional to $\mathcal{C}_1$ even if $|\alpha|$ is small enough, see Fig. 5(a) and 5(b). The robustness of $\delta\tilde{N}$ against small perturbations is also demonstrated in Figs. 5(c)–5(f). The rotation angle $\theta_1$ is also chosen randomly from the interval $[\bar{\theta}_1 - \frac{\pi}{20}, \bar{\theta}_1 + \frac{\pi}{20}]$ at every step of our DTQW, with $\bar{\theta}_1$ indicating the corresponding parameter without disorder. Here the strength of decoherence is chosen as $q = 0.01$.

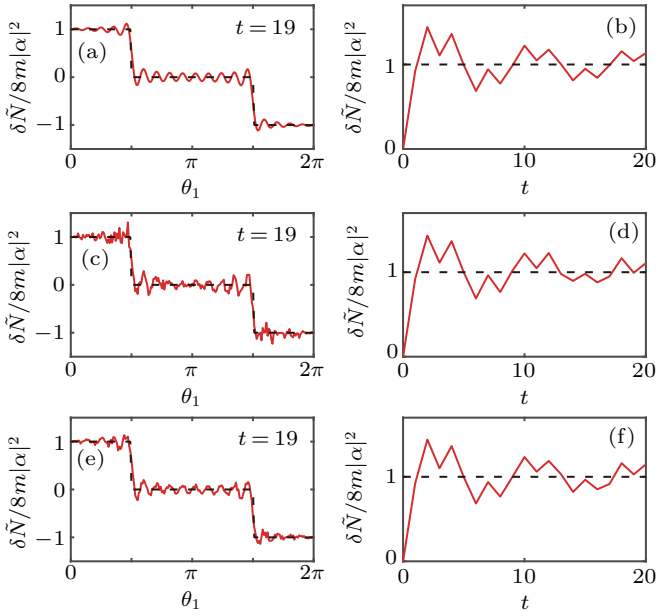


**Fig. 5.** The combination of the average projective phonon numbers $\delta\tilde{N}$ governed by $\tilde{U}_{1}^{\alpha}$. The dashed lines correspond to the topological invariant $\nu_1/2$ governed by $U_1$. (a) The combination of the average projective phonon numbers $\delta\tilde{N}$ as a function of the rotation angle $\theta_1$ with $t = 19$, $\theta_2 = 3\pi/2$ and $|\alpha| = 0.3$. (b) The combination of the average projective phonon numbers $\delta\tilde{N}$ as a function of the step $t$ with $|\alpha| = 0.3$, $\theta_2 = 3\pi/2$ and $\theta_1 = \pi/4$. For the situation with (c), (d) dynamical disorder or (e), (f) decoherence, the solid lines indicate the ensemble average over 50 times of DTQWs with dynamical disorder or decoherence.

In a realistic ion-trap experiment,[58] the phonon number can be detected varying with the interaction time. In other ion-trap experiments for realizing DTQWs,[20,21] the system can be detected at different steps of DTQWs. Thus, the measurement of the projective phonon numbers at different steps of DTQWs proposed in our scheme is possible in current ion-trap techniques.

## 5. Conclusion

In summary, we have proposed experimental protocols to realize topological DTQWs in the system of single trapped

ion, where the walk takes place in coherent state space. We demonstrate that the experimental measurement of bulk topological features can be easily monitored through the average projective phonon number. No more experimental technologies for reading out all position states or tomography are required. In addition, the chiral symmetry owned by our DTQWs further simplifies the experimental measurement process. By introducing dynamical disorder and decoherence, we verify the robustness of our results. This work gives a simple method to directly measure bulk topological invariants using discrete-time quantum dynamics of in coherent state space.

## Appendix A

We denote the $j+1$-th term in Eq. (20) as $\tilde{\mathcal{T}}_j^{\uparrow\downarrow}(j\neq 0)$ and it can be written in the following form:

$$\begin{aligned}\tilde{\mathcal{T}}_j^{\uparrow\downarrow} &= |\alpha|^2 \mathrm{e}^{-j^2|\alpha|^2/2}\langle\Psi_f|x(\mathrm{e}^{\mathrm{i}(j\phi)}\mathrm{e}^{\mathrm{i}kj} \\ &\quad + \mathrm{e}^{-\mathrm{i}(j\phi)}\mathrm{e}^{-\mathrm{i}kj})x|\uparrow\downarrow\rangle\langle\uparrow\downarrow||\Psi_f\rangle \\ &= 2|\alpha|^2\mathrm{e}^{-j^2|\alpha|^2/2}\{\cos(j\phi)\langle\Psi_f|x\cos(kj)x|\uparrow\downarrow\rangle\langle\uparrow\downarrow||\Psi_f\rangle \\ &\quad - \sin(j\phi)\langle\Psi_f|x\sin(kj)x|\uparrow\downarrow\rangle\langle\uparrow\downarrow||\Psi_f\rangle\}, \end{aligned} \tag{A1}$$

where $|\Psi_f\rangle = \sum_{x,\sigma}A_{x,\sigma}|x\rangle$ indicates the final state of DTQW governed by $U_1$. Following Eq. (A1) to calculate $\tilde{N}^{\uparrow\downarrow}$, we have

$$\begin{aligned}\tilde{N}^{\uparrow\downarrow} &= |\alpha|^2\sum_x x^2|A_{x,\uparrow\downarrow}|^2 \\ &\quad - 2|\alpha|^2\sum_{m=1}^{\infty}\mathrm{e}^{-m^2|\alpha|^2/2}\{\cos(m\phi)\mathcal{L}^{\uparrow\downarrow}(m) \\ &\quad - \sin(m\phi)\mathcal{R}^{\uparrow\downarrow}(m)\}t^2, \end{aligned} \tag{A2}$$

where

$$\mathcal{L}^{\uparrow\downarrow}(m) \equiv \int_{-\pi}^{\pi}\frac{\mathrm{d}k}{2\pi}\langle\varphi_0|U_1^{-t}\frac{\partial}{\partial k}\cos(mk)\frac{\partial}{\partial k}|\uparrow\downarrow\rangle\langle\uparrow\downarrow|U_1^t|\varphi_0\rangle/t^2,$$

$$\mathcal{R}^{\uparrow\downarrow}(m) \equiv \int_{-\pi}^{\pi}\frac{\mathrm{d}k}{2\pi}\langle\varphi_0|U_1^{-t}\frac{\partial}{\partial k}\sin(mk)\frac{\partial}{\partial k}|\uparrow\downarrow\rangle\langle\uparrow\downarrow|U_1^t|\varphi_0\rangle/t^2.$$

In the long-time limit $t\to\infty$, by ignoring infinitesimal terms, $\mathcal{L}^{\uparrow\downarrow}(m)$ have the form

$$\begin{aligned}\mathcal{L}^{\uparrow\downarrow}(m) &\approx \int_{-\pi}^{\pi}\frac{\mathrm{d}k}{2\pi}\cos(mk)\left(\frac{\mathrm{d}E}{\mathrm{d}k}\right)^2 \\ &\quad\times\left\{-\frac{1}{2}\mp\frac{1}{2}\cos(2Et)(|s_\uparrow|^2-|s_\downarrow|^2)\right. \\ &\quad\pm\frac{\mathrm{i}}{2}\sin(2Et)n_x(s_\uparrow^*s_\downarrow - s_\downarrow^*s_\uparrow) \\ &\quad\left.\pm\frac{1}{2}\sin(2Et)n_y(s_\uparrow^*s_\downarrow + s_\downarrow^*s_\uparrow)\right\}, \end{aligned} \tag{A3}$$

where $s_\uparrow = \langle\uparrow|\varphi_0\rangle$ and $s_\downarrow = \langle\downarrow|\varphi_0\rangle$. We further ignore the last three terms in Eq. (A3) since they only plus oscillatory contributions whose amplitude and period generally decay rapidly as $t\to\infty$. Thus, we can arrive at

$$\begin{aligned}\mathcal{L}^{\uparrow\downarrow}(m) &\approx -\frac{1}{2}\int_{-\pi}^{\pi}\frac{\mathrm{d}k}{2\pi}\cos(mk) \\ &\quad\times\frac{2\sin^2\left(\frac{\theta_1}{2}\right)\sin^2(2k)}{1-\frac{1}{2}\left(\sin\frac{\theta_1}{2}\cos(2k)+\cos\frac{\theta_1}{2}\right)^2}, \end{aligned} \tag{A4}$$

which satisfies $\mathcal{L}^{\uparrow\downarrow}(m=\text{odd})=0$. Furthermore, $\mathcal{R}^{\uparrow\downarrow}(m)=0$ for all $m$, since the integrand for calculating $\mathcal{R}^{\uparrow\downarrow}(m)$ is an odd function for $k$.

## References


[1] Hasan M Z and Kane C L 2010 *Rev. Mod. Phys.* **82** 3045
[2] Qi X L and Zhang S C 2011 *Rev. Mod. Phys.* **83** 1057
[3] Chiu C K, Teo J C Y, Schnyder A P and Ryu S 2016 *Rev. Mod. Phys.* **88** 035005
[4] Sheng D N, Weng Z Y, Sheng L and Haldane F D M 2006 *Phys. Rev. Lett.* **97** 036808
[5] Lu L, Joannopoulos J D and Soljačić M 2014 *Nat. Photon.* **8** 821
[6] Lu L, Joannopoulos J D and Soljačić M 2016 *Nat. Phys.* **12** 626
[7] Ozawa T, Price H M, Amo A *et al.* 2019 *Rev. Mod. Phys.* **91** 015006
[8] Goldman N, Budich J C and Zoller P 2016 *Nat. Phys.* **12** 639
[9] Dauphin A and Goldman N 2013 *Phys. Rev. Lett.* **111** 135302
[10] Atala M, Aidelsburger M, Barreiro J T, Abanin D, Kitagawa T, Demler E and Bloch I 2013 *Nat. Phys.* **9** 795
[11] Jotzu G, Messer M, Desbuquois R, Lebrat M, Uehlinger T, Greif D and Esslinger T 2014 *Nature* **515** 237
[12] Aidelsburger M, Lohse M, Schweizer C, Atala M, Barreiro J T, Nascimbene S, Cooper N R, Bloch I and Goldman N 2015 *Nat. Phys.* **11** 162
[13] Fläschner N, Rem B S, Tarnowski M, Vogel D, Lühmann D S, Sengstock K and Weitenberg C 2016 *Science* **352** 1091
[14] Mittal S, Ganeshan S, Fan J Y, Vaezi A and Hafezi M 2016 *Nat. Photon.* **10** 180
[15] Aharonov Y, Davidovich L and Zagury N 1993 *Phys. Rev. A* **48** 1687
[16] Kitagawa T, Rudner M S, Berg E and Demler E 2010 *Phys. Rev. A* **82** 033429
[17] Kitagawa T 2012 *Quantum Inf. Process.* **11** 1107
[18] Karski M, Forster L, Choi J M, Steffen A, Alt W, Meschede D and Widera A 2009 *Science* **325** 174
[19] Genske M, Alt W, Steffen A, Werner A H, Werner R F, Meschede D and Alberti A 2013 *Phys. Rev. Lett.* **110** 190601
[20] Schmitz H, Matjeschk R, Schneider C, Glueckert J, Enderlein M, Huber T and Schaetz T 2009 *Phys. Rev. Lett.* **103** 090504
[21] Zähringer F, Kirchmair G, Gerritsma R, Solano E, Blatt R and Roos C F 2010 *Phys. Rev. Lett.* **104** 100503
[22] Schreiber A, Cassemiro K N, Potoček V, Gábris A, Mosley P J, Andersson E, Jex I and Silberhorn C 2010 *Phys. Rev. Lett.* **104** 050502
[23] Broome M A, Fedrizzi A, Lanyon B P, Kassal I, Aspuru-Guzik A and White A G 2010 *Phys. Rev. Lett.* **104** 153602
[24] Ryan C A, Laforest M, Boileau J C and Laflamme R 2005 *Phys. Rev. A* **72** 062317
[25] Asbóth J K 2012 *Phys. Rev. B* **86** 195414
[26] Asbóth J K and Obuse H 2013 *Phys. Rev. B* **88** 121406
[27] Tarasinski B, Asbóth J K and Dahlhaus J P 2014 *Phys. Rev. A* **89** 042327
[28] Obuse H, Asbóth J K, Nishimura Y and Kawakami N 2015 *Phys. Rev. B* **92** 045424
[29] Edge J M and Asbóth J K 2015 *Phys. Rev. B* **91** 104202
[30] Asbóth J K 2015 *Phys. Rev. A* **91** 022324
[31] Rakovszky T and Asbóth J K 2015 *Phys. Rev. A* **92** 052311
[32] Groh T, Brakhane S, Alt W, Meschede D, Asbóth J K and Alberti A 2016 *Phys. Rev. A* **94** 013620
[33] Mugel S, Celi A, Massignan P, Asbóth J K, Lewenstein M and Lobo C 2016 *Phys. Rev. A* **94** 023631
[34] Rakovszky T, Asbóth J K and Alberti A 2017 *Phys. Rev. B* **95** 201407
[35] Ramasesh V V, Flurin E, Rudner M, Siddiqi I and Yao N Y 2017 *Phys. Rev. Lett.* **118** 13050
[36] Sajid M, Asbóth J K, Meschede D, Werner R F and Alberti A 2019 *Phys. Rev. B* **99** 214303

[37] Kitagawa T, Broome M A, Fedrizzi A, Rudner M S, Berg E, Kassal I, Aspuru-Guzik A, Demler E and White A G 2012 *Nat. Commun.* **3** 882
[38] Cardano F, Maffei M, Massa F, Piccirillo B, Lisio C D, Filippis G D, Cataudella V, Santamato E and Marrucci L 2016 *Nat. Commun.* **7** 11439
[39] Cardano F, D'Errico A, Dauphin A *et al.* 2017 *Nat. Commun.* **8** 15516
[40] Barkhofen S, Nitsche T, Elster F, Lorz L, Gábris A, Jex I and Silberhorn C 2017 *Phys. Rev. A* **96** 033846
[41] Flurin E, Ramasesh V V, Hacohen-Gourgy S, Martin L S, Yao N Y and Siddiqi I 2017 *Phys. Rev. X* **7** 031023
[42] Xu Y X, Wang Q Q, Pan W W *et al.* 2018 *Phys. Rev. Lett.* **120** 260501
[43] Xiao L, Zhan X, Bian Z H *et al.* 2017 *Nat. Phys.* **13** 1117
[44] Zhan X, Xiao L, Bian Z H, Wang K K, Qiu X Z, Sanders B C, Yi W and Xue P 2017 *Phys. Rev. Lett.* **119** 130501
[45] Xiao L, Qiu X Z, Wang K K, Bian Z H, Zhan X, Obuse H, Sanders B C, Yi W and Xue P 2018 *Phys. Rev. A* **98** 063847
[46] Wang K K, Qiu X Z, Xiao L, Zhan X, Bian Z H, Sanders B C, Yi W and Xue P 2019 *Nat. Commun.* **10** 2293
[47] Wang K K, Qiu X Z, Xiao L, Zhan X, Bian Z H, Yi W and Xue P 2019 *Phys. Rev. Lett.* **122** 020501
[48] Xiao L, Wang K K, Zhan X, Bian Z H, Kawabata K, Ueda M, Yi W and Xue P 2019 *Phys. Rev. Lett.* **123** 230401
[49] Wang B, Chen T and Zhang X 2018 *Phys. Rev. Lett.* **121** 100501
[50] Chen C, Ding X, Qin J *et al.* 2018 *Phys. Rev. Lett.* **121** 100502
[51] Chalabi H, Barik S, Mittal S, Murphy T E, Hafezi M and Waks E 2019 *Phys. Rev. Lett.* **123** 150503
[52] Ge Z Y and Fan H 2018 arXiv:1804.06994v2[hep-ph] [quant-ph]
[53] Xue P, Sanders B C and Leibfried D 2009 *Phys. Rev. Lett.* **103** 183602
[54] Leibfried D, Blatt R, Monroe C and Wineland D 2003 *Rev. Mod. Phys.* **75** 281
[55] Brownnutt M, Kumph M, Rabl P and Blatt R 2015 *Rev. Mod. Phys.* **87** 1419
[56] Harlander M, Lechner R, Brownnutt M, Blatt R and Hänsel W 2011 *Nature* **471** 200
[57] Brown K R, Ospelkaus C, Colombe Y, Wilson A C, Leibfried D and Wineland D J 2011 *Nature* **471** 196
[58] Maslennikov G, Ding S, Hablützel R, Gan J, Roulet A, Nimmrichter S, Dai J, Scarani V and Matsukevich D 2019 *Nat. Commun.* **10** 202
[59] Xu Y Y, Zhou F, Chen L, Xie Y, Xue P and Feng M 2012 *Chin. Phys. B* **21** 040304
[60] Kim K, Chang M S, Korenblit S, Islam R, Edwards E E, Freericks J K, Lin G D, Duan L M and Monroe C 2010 *Nature* **465** 590
[61] Alberti A, Alt W, Werner R and Meschede D 2014 *New J. Phys.* **16** 123052